16th Australasian Fluid Mechanics Conference
Crown Plaza, Gold Coast, Australia
2-7 December 2007

Interaction of an unequal-strength vortex pair

J. So[1], K. Ryan[1] and G. J. Sheard[1,2]

[1]Fluids Laboratory for Aeronautical and Industrial Research (FLAIR),
Department of Mechanical Engineering, Monash University, VIC 3800, AUSTRALIA

[2]Monash University Biomedical Engineering Alliance (MuBeta),
Monash University, VIC 3800, AUSTRALIA

Abstract

In this investigation, two-dimensional simulations of unequal strength Lamb–Oseen counter-rotating vortex pairs were conducted using a spectral-element method. Simulations were performed at three different Reynolds numbers, $Re = 6660$, 13340 and 20000, and various relative strength of vortex circulation ratios were considered. The strain adaptation and the viscous relaxation were shown to be dependent on the relative strength of the vortices, but independent of Reynolds number. The vortex pairs converged to a unique solution on the viscous time-scale for each relative strength value. The completion of the adaptation and the relaxation are determined based on the variation of the vortex eccentricity which is a ratio of the strain rate to the vorticity at each vortex center. The viscosity begins to affect the vortex dynamics once those two processes are completed.

The two-dimensional simulation results also provide the initial base flows of vortex pairs which will be used in future three-dimensional stability analysis studies.

Introduction

The phenomenon of self adaptation of a vortex dipole acting under a mutually induced strain field has been discussed in previous studies of Moore and Saffman [9] and Ting and Klein [12]. In numerical simulations of the vortex pair problems, the two mechanisms comprising self adaptation (namely inviscid and viscous adaptation) are essential to alter vortex pairs with any profiles (e.g. Rankine vortex and Lamb–Oseen vortex) toward the quasi-steady solution of the Navier–Stokes equations.

Vortex pair formation

When a vortex pair forms, it gradually settles itself by two mechanisms; the first one is the strain adaptation and the second is the viscous relaxation (Sipp *et al.* [11]). Although these two mechanisms are discussed separately, the current investigation will not define the time of transition between the two.

The first stage requires two vortices to adapt to the induced strain from its counterpart. This adaptation has been shown to be an inviscid process (Le Dizès and Verga [6]), as strain is the dominant mechanism. This process involves the modification of the flow structure of each vortex, from axisymmetric to an elliptic form. This was first addressed in Moore and Saffman [9] who considered the time evolution of the stream-function of a vortex under strain.

The second stage is a viscous relaxation. A vortex pair with two identical circular vortices will evolve towards a physical solution of the Navier–Stokes equations, where each vortex has an elliptic cross section. Beyond this, each vortex radius will grow over time due to viscous dissipation. Batchelor [1] developed an equation to evaluate the viscous evolution of the radius as a function of time

$$a = \sqrt{a_o^2 + 4\nu t}, \tag{1}$$

where ν is the viscosity of the fluid and t is the time scale.

Equal strength vortex pairs

Previous research has investigated the self adaptation of vortex pairs in a two-dimensional flow with equal circulation strength for both co-rotating or counter-rotating orientation (Sipp *et al.* [11], Le Dizès and Verga [6]). Various vortex profiles have been considered. The important finding is that the strain adaptation and the viscous relaxation of a vortex pair are independent of Reynolds number.

Vortex pairs under different viscous effects have been shown to evolve to a unique dipole solution which can be described by a spacing ratio, a/b; of the vortex effective radius, a to the vortex separation, b (Sipp *et al.* [11]).

Different evolution behavior of various vortex profiles have been described by measuring the vortex deformation. Sipp *et al.* [11] used the vortex aspect ratio of the deformed vortex whereas Le Dizès and Verga [6] defined two vortex eccentricities referred to as the local and global eccentricities. The vortex deformation here was monitored by computing the local eccentricity which measures the deformation of the flow-field stream-function at the vortex core (Le Dizès and Verga [6]). Here the eccentricity, ε_i, was defined as the ratio of internal strain rate, S_i, with the angular velocity at the vortex core (defined by Le Dizès and Verga [6] as half of the core vorticity). The internal strain rate is different from the external strain as the external one ignores the influence from the interaction between the vorticity and the strain (Le Dizès and Verga [6]). Thus the choice of the local eccentricity is more representative for the purpose of this investigation.

Beside the spacing ratio of a/b and the deformation scale of ε_i; another ratio which describes the vortices relative circulation is defined as Λ; (the weaker vortex circulation divided by the stronger vortex circulation). In general, Λ is negative for counter-rotating vortex pairs and positive for co-rotating pairs, $|\Lambda| = 1$ denotes an equal strength (even) vortex pair.

An even vortex pair deforms co-operatively due to the exposure of the equal induced strain. Previous observations described such deformation as an elliptic deformation (Leweke and Williamson [5], Meunier *et al.* [8]); (though the vortex pair alignments are different for the co-rotating and the counter-rotating cases). A co-rotating pair is observed to merge due to the radius growing by viscous diffusion which increases the value of a/b to the point where merging occurs. Due to this, the current investigation only focuses on counter-rotating vortex pairs.

Unequal strength vortex pairs

By comparison with equal strength vortex pairs, relatively little work has been conducted considering vortex pairs with unequal circulations. Ortega *et al.* [10] experimentally considered unequal-strength counter-rotating vortex pairs formed from particular wing platforms. Three-dimensional instabilities of the vortex pairs were observed, however the structures and the instability mechanisms driving the growth of the vortex pairs were not described in detail. Bristol *et al.* [2] conducted a similar study of unequal strength vortex pairs analytically and numerically. Co-rotating cases were also considered. The instability growth rates and the wavenumbers were predicted by a theoretical model and were compared with the results of the numerical simulations. Self-adaptations and the deformations of the unequal strength vortices used in their numerical validation were not addressed.

By considering only specific planforms, the work of Ortega *et al.* [10] was restricted to particular values of Λ and Reynolds number. This limited the general observations they could make on the instability process affecting the vortex pair. By considering the strain response of an unequal strength vortex pair, this investigation serves as the basis for a wider parameter study which will provide a more general understanding of the physical mechanisms underpinning dissipation of unequal strength vortex pairs.

Unequal strength vortex pairs commonly appear in engineering flows. One typical example is the vortices from the trailing edge of an aircraft wing. This area is one of active research in the aviation industry. Although such vortex pairs are three-dimensional, thorough understanding of the two-dimensional vortex dynamics underpinning these flows is essential, and is the focus of the present study. The dependence of the relative strength and the independence of the Reynolds numbers are described. The self-adaptation and the viscous relaxation for a range of vortex pair circulations ($\Lambda \in [-1,-0.1]$) are addressed and compared.

Simulation flow description

The initial base flow was constructed by super-imposing two Lamb–Oseen vortices with equal radius and an initial spacing ratio of $a/b = 0.25$.A schematic representation of the pair geometry is shown in figure 1.

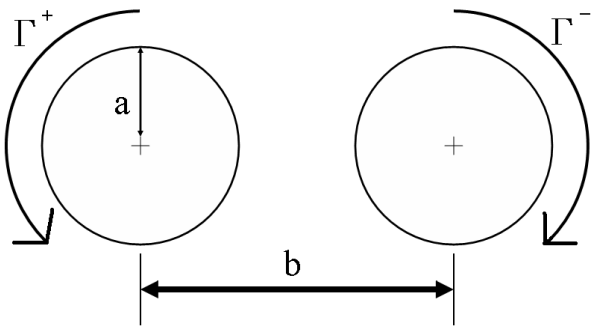

Figure 1: Schematic diagram of a vortex pair

For all simulations, the circulation-based Reynolds number, Re $(=\Gamma/\nu)$ was set to 6660, 13340 or 20000, respectively. The vorticity equation of a Lamb-Oseen vortex in cylindrical coordinates based on the vortex center is

$$\omega_{axial} = \frac{\Gamma}{\pi a_\circ^2} e^{-(\frac{r}{a_\circ})^2}, \tag{2}$$

where Γ is the vortex circulation and ω_{axial} is the vorticity on $X-Y$ plane; r is the radius dimension and $a_\circ$ is the initial radius of a vortex. This equation is resolved into the x and y components in the numerical model. The positive vortex strength is held constant at, $\Gamma^+ = 3\pi$. The negative vortex circulation, Γ^-, was equivalent to the product of the Λ and the positive vortex circulation. Λ $(\in [-1,-0.1])$ has increments of 0.045.

For an even vortex pair, a self-induced velocity of $U = \Gamma/2\pi b$ propels the pair in a direction perpendicular to the line connecting the vortex centers. However, the self-induced velocity of an uneven pair is not similarly translational because of the difference of the circulation strengths. Considering two point vortices, the induced velocity is $U^+ = \Gamma^-/2\pi b$ on the positive vortex and $U^- = \Gamma^+/2\pi b$ on the negative vortex. The resultant velocity of the pair, $U_{Resultant}$, can be approximated linearly as a function of Γ^+, Γ^- and b along the line joining two vortices. A moving reference frame was applied in the simulations to confine the vortex pair movement within the center of the grid. The details are provided in the numerical formulation section.

Eccentricity and internal strain

We define the eccentricity as a ratio of the internal strain rate, S_i to the magnitude of the half vorticity, $|\omega_{axial}|/2$ at the vortex center. Following the work of Le Dizès and Verga [6]. This eccentricity is appropriate to describe how the flow streamfunction is adjusted due to the induced strain around the vortex core from its counterpart because of the involved internal strain which quantifies the interaction between the strain and the vorticity around the core. The equations for computing the vorticity (3) in the simulations and the the strain rate tensor (4) are

$$\omega_{axial} = \left(\frac{\partial v}{\partial x} - \frac{\partial u}{\partial y}\right), \tag{3}$$

$$\begin{aligned} \tilde{\tau} &= \frac{1}{2}\left(\frac{\partial u_i}{\partial x_j} + \frac{\partial u_j}{\partial x_i}\right), \\ &= \begin{bmatrix} \frac{\partial u}{\partial x} & \frac{1}{2}\left(\frac{\partial u}{\partial y} + \frac{\partial v}{\partial x}\right) \\ \frac{1}{2}\left(\frac{\partial u}{\partial y} + \frac{\partial v}{\partial x}\right) & \frac{\partial v}{\partial y} \end{bmatrix}, \end{aligned} \tag{4}$$

where u and v are the flow field components. The strain rate magnitude (principal strain ratio) is equal to the largest eigenvalue of $\tilde{\tau}$. The direction of this principal strain rate is parallel to the corresponding eigenvector of this eigenvalue. Herein strain is referred to as the internal strain which is measured at the vortex center.

Numerical formulation

A spectral-element method was used in this direct numerical simulation investigation. High-order Lagrangian polynomials were employed as the interpolation scheme within each macro element. A third-order accurate backwards multi-step time integration scheme was applied. Details of the scheme are provided in Karniadakis *et al.* [7]. The spatial accuracy is dependent on the order of Lagrangian polynomials within each element. A grid independence study was performed which monitored the convergence of the eccentricity and the instantaneous vortex circulations.

The mesh has 441 macro elements and the simulations have been performed at two resolutions. The lower resolution mesh employed 10^{th}- order polynomials within each element. Lower resolution computations have been completed for 200 computational time units. The flow-field has been sufficiently resolved for the self-adaptation and the viscous relaxation. However, a few results showed that the uneven vortex pair interaction is sensitive with the strength difference when Λ is close to -0.1. Moreover, for simulations at high Reynolds number (up to 20000) high numerical noise was observed. These simulations have been recomputed at a higher resolution mesh with 13^{th}- order polynomials, but they were only computed up to 100 time units. The vortex interaction up to that point is well beyond the adaptation and the relaxation completion so that the physics describing the vortex interaction have already been captured.

The domain is a square of length l where l is 100 times the vortex initial radius, $a_\circ$. A picture of the grid is shown in figure 2. This domain size has been validated by a domain analysis; that the domain is sufficiently large for the vorticity at the boundaries to be negligible, as the vorticity is an exponential function in equation (2).

Grid features & Moving reference

The grid is sufficiently refined at its center for the physics underlying the motion of the vortex pairs to be captured. A narrow layer of elements is aligned with the the domain boundaries. This layer was found to minimise the generation of spurious vorticity due to the interaction between the imposed time-dependent boundary velocities and the small finite velocities propagated from the pair.

The instantaneous center of the rotational motion is located by a linear function of Γ^+, Γ^- and b. If only the resultant translational component of the positive vortex is subtracted from the velocity field, the negative vortex can still rotate around the positive vortex but the pair cannot move out of the refined computational domain. This moving reference mechanism is implemented when the mesh boundaries are defined as time-dependent boundaries. The translational velocity component of the positive vortex is subtracted over the whole computational domain but imposed against that component along all the boundaries to balance the motion.

Results – Unequal strength vortex pairs

Having described the formation and the interaction of general vortex pairs, this section now considers unequal strength vortex pairs. The unequal strength vortex pairs were considered (with $\Lambda = -0.1$, -0.37 and -0.73) and compared with an equal strength vortex pair ($\Lambda = -1.0$). The unequal strength vortex pairs were seen to interact differently to an equal strength pair. The major differences are summarised as the following points:

(a) Uneven vortices rotated around each other because of the unequal induced velocities, the rotational motion is similar to co-rotating vortex pairs but without merging consequently.

(b) The relative rotational speed was found to be inversely dependent on the relative strength of the vortices, Λ.

(c) The vortex pair experienced asymmetric deformation because of the unequal induced strains. In this current investigation, the deformation of the negative vortex increased when Λ decreased toward -0.1, whereas the positive vortex deformation decreased.

(d) The deformation time-scale of each vortex differed from the other.

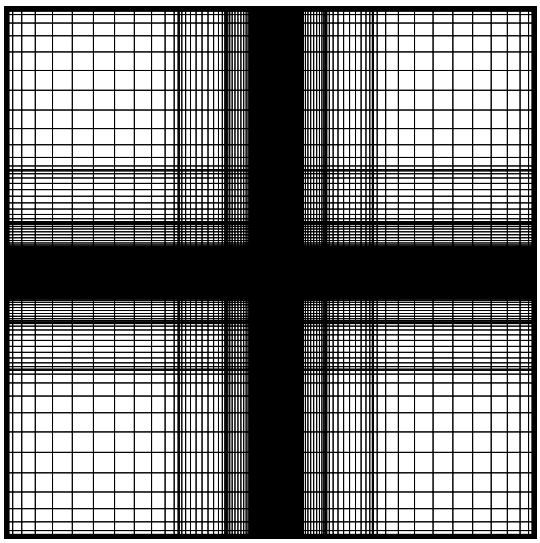

Figure 2: The spectral element mesh; the square domain has side length $100a$.

Four vorticity contour snapshots from the simulations computed at Re $= 20000$ are presented in figure 3 for $\Lambda = -0.1$, -0.37, -0.73 and -1.0. These snapshots were all captured at $t^*_{vis} = 0.015$ on the viscous time scale ($= t\nu/\pi a_o^2$). Each vortex pair at this stage has reached steady state far beyond the strain adaptation phase, but the vortex pair evolution continues due to the viscous effect described in the literature as viscous relaxation.

The reference $\Lambda = -1.0$ pair deformed symmetrically into an elliptic vortex pair. The $\Lambda = -0.73$ pair deformed asymmetric, and rotation of the vortices occurred. The asymmetric deformation became obvious when $|\Lambda|$ was decreased. The $\Lambda = -0.37$ and the -0.1 cases show a contrast in the topology. For $\Lambda = -0.37$, the positive vortex deformed slightly in its weak vorticity region but the core remained comparatively circular. On the other hand, the negative vortex was stretched angularly and compressed radially with respect to the positive vortex center. The biggest deformation is the most extreme Λ case. For the $\Lambda = -0.1$ pair, the entire positive vortex remained relatively circular while the negative vortex deformed extensively. The rotational speed increased with the increment in Λ. Table 1 gives the instantaneous eccentricity values of the vortices shown in figure 3.

Instantaneous Eccentricity – ε_i ($t^*_{vis} = 0.015$)				
Λ	-0.1	-0.37	-0.73	-1.0
Positive vortex	0.012	0.063	0.126	0.170
Negative vortex	1.233	0.407	0.226	0.170

Table 1: Instantaneous eccentricity, ε_i of the vortices of the pairs with different $\Lambda = -0.1$, -0.37, -0.73 and -1.0; Results computed at $t^*_{vis} = 0.015$ on the viscous time scale, Reynolds number $= 20000$.

Results – Strain adaptation

The strain adaptation phase involved the modification of the flow structure surrounding the vortices to adapt the induced strain from its counterpart. From the work of Le Dizès and Verga [6], the co-rotating vortices deform due to the strain in the vortex cores and the weaker vorticity regions. But the de-

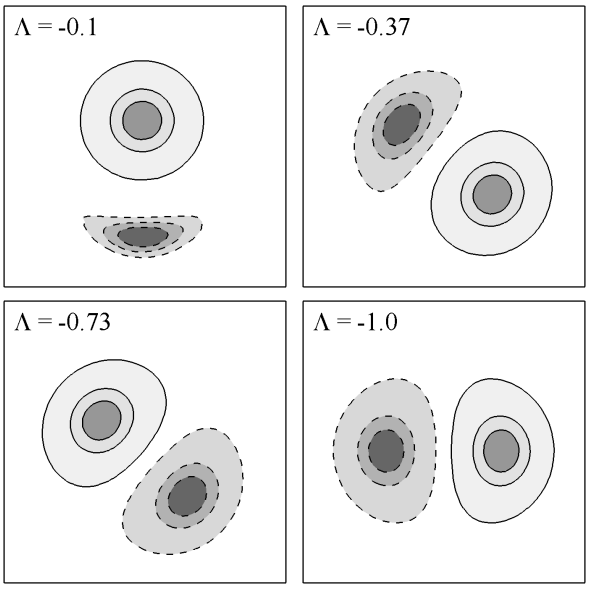

Figure 3: Vorticity contour snapshots of $\Lambda = -0.1$, -0.37, -0.73 and -1.0. $Re = 20000$. Solid and dashed lines show positive and negative vorticity, respectively, and contour levels are arbitrary.

formation process is not uniform across the vortex. The weaker vorticity region experienced more complicated flow interaction and became more elliptic than the core.

Similar interactions were observed in our simulations. However, the modification of the flow structure around the negative and the positive vortices were not alike because of the unequal induced strains. In particular, the deformation magnitudes and deformation time-scales of the vortices were different. In figure 4, a time-series snapshot of the simulation of $\Lambda = -0.415$ at a lower Reynolds number $= 13340$ illustrates the flow structure evolution during the strain adaptation phase. The direction of the principal strain at each vortex center is also displayed. The time-series show is from the beginning of the simulation until the flow interaction between the two vortices was settled. The settlement of the flow was monitored by the oscillation of the eccentricity shown in figure 7 which is at $t^*_{vis} = \approx 7.5e-3$. The moment is determined by the amplitude of the eccentricity to be within 1% of the mean eccentricity.

The flow modification begins with the negative vortex pulled around the positive vortex and deformed. The core of the negative vortex rapidly deforms into a elliptic shape while the positive core remains relative circular. The weaker vorticity regions of both vortices displayed elliptic deformation ($t^*_{vis} = 0.67e-3$ & $1.35e-3$). The negative vortex evolved more rapidly. Vortex filaments were observed to emanate from the vortex core of each vortex ($t^*_{vis} = 2.70e-3$, $3.60e-3$ & $4.72e-3$). The filament emanation is stronger from the negative vortex which is under a stronger induced strain. These filaments were observed to decay rapidly. The outer region of the positive vortex became steady earlier as the emanation eased when some unsteady activities occurred around the negative vortex ($t^*_{vis} = 5.85e-3$ & $6.75e-3$). At the last three snapshots ($t^*_{vis} = 7.65e-3$ & $9.45e-3$), the vortex pair have formed into an asymmetric elliptic vortex pair which is similar to the example in figure 3 of $\Lambda = -0.37$.

The principal strain direction for both vortices was observed to be maintained at around $\pm 45^\circ$ with respect to the imagined line

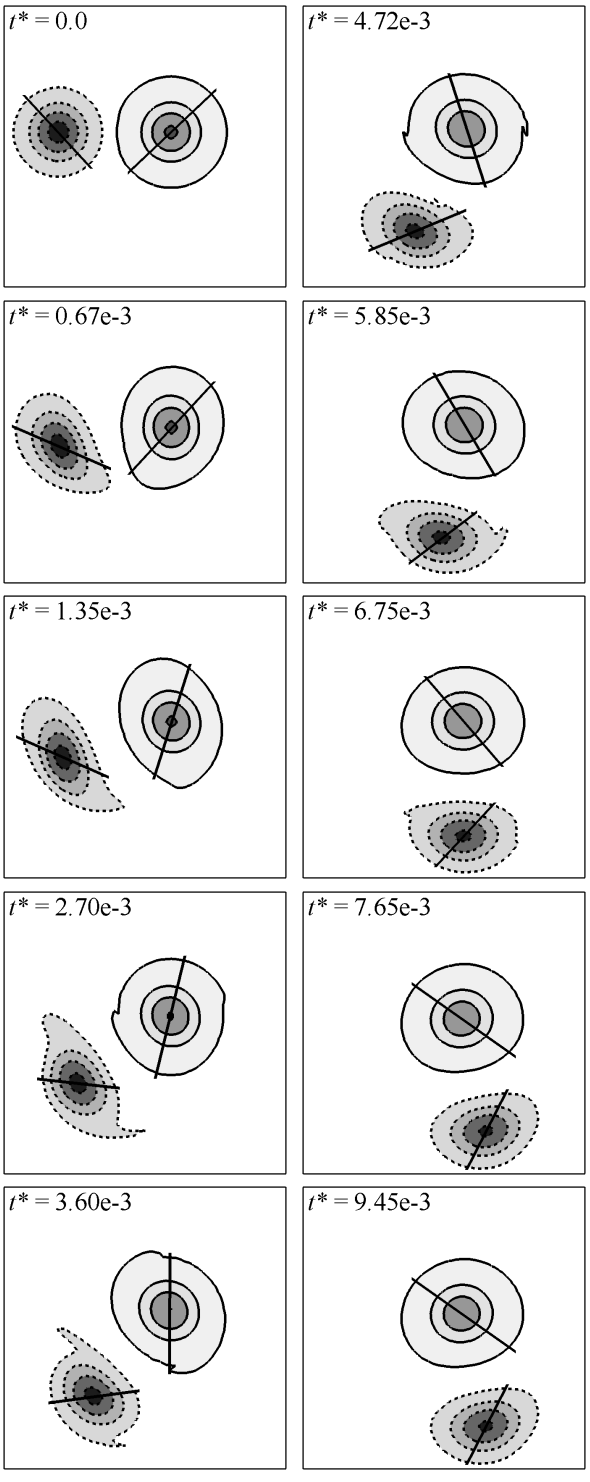

Figure 4: Snapshots of a $\Lambda = -0.415$ vortex pair evolution during the strain adaptation on the viscous time scale. $Re = 13340$. Contour lines and shading is as per Figure 3.

connecting two vortices. Although it varied slightly at $t^*_{vis} = 0.67e-3$ & $1.35e-3$, it gradually settles to about $\pm 45^\circ$ orientation. The rotational motion does not appear to impact the strain direction. The strain, the vorticity and the eccentricity of the $\Lambda = -0.415$ pair shown in figure 4 were plotted on the viscous time scale ($Re = 13340$) in figure 5, 6 and 7.

The peak vorticity of each vortex throughout the simulation de-

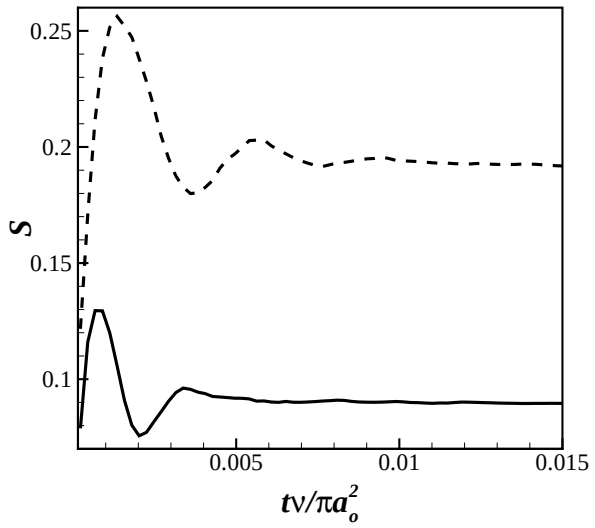

Figure 5: Strain of $\Lambda = -0.415$ vortex pair plotted against the viscous time scale, $Re = 13340$. The solid line represents the positive vortex and the dashed line is negative.

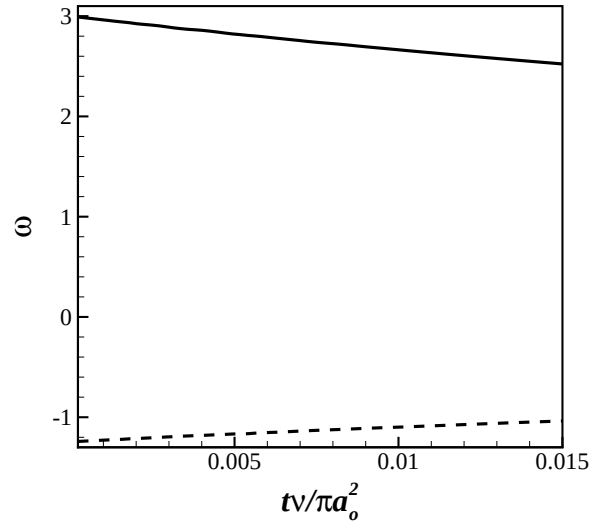

Figure 6: Vorticity of $\Lambda = -0.415$ vortex pair plotted against the viscous time scale, $Re = 13340$. The solid line represents the positive vortex and the dashed line is negative.

cayed due to viscosity as shown in figure 6. The vorticity decay rates, $\partial\omega/\partial t^*_{vis}$ are computed to be $|32.21|$ for the positive vortex and $|13.56|$ for the negative vortex. Both curves are assumed to be linear. The strain curves in figure 5 show a similar trend to the eccentricity curves shown in figure 7. Both figures begin with overshoots for the vortices and then become steady in a linear trend. The overshoots on both figures correspond to each other (following from the vorticities constantly decay with time from the beginning). Therefore, it is reasonable to state that the first stage of the vortex pair interaction must be dominated by the strain instead of the viscous effect. Although the eccentricity here is mainly concerned about the vortex core and does not take account of the mean vortex structure changes, the authors have assumed that the difference between the local and the global eccentricities was small as the vortices are concentrated in this investigation.

Moreover, the modification of the flow has different time scales

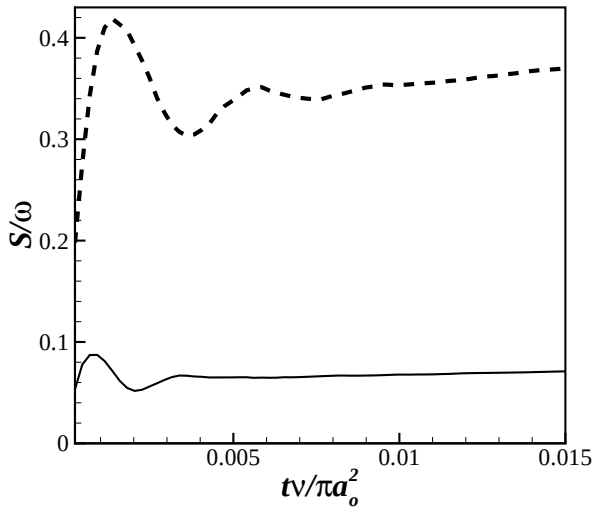

Figure 7: Eccentricity of $\Lambda = -0.415$ vortex pair plotted against the viscous time scale, $Re = 13340$. The solid line represents the positive vortex and the dashed line is negative.

for each vortex in the unequal strength pair. In figure 7, oscillations of the negative vortex eccentricity are maintained for longer and have larger amplitudes. The oscillation duration is consistent with the vorticity contour snapshots that relatively stronger activities occurred in the negative vortex and they took longer to settle.

Results – Viscous relaxation

After the strain adaptation, the viscous effect dominated the flow evolution. Previous work has shown that the viscous effect can modify any vortex type toward the common quasi-steady solution of the Euler equation, the Gaussian vortex (Sipp *et al.* [11] and Le Dizès and Verga [6]). By choosing a Lamb–Oseen vortex profile, we have avoided considering the effect of any non-Gaussian vortex on the adaptation and relaxation. The Lamb-Oseen vortex is a vortex with Gaussian profile.

The evolution of the unequal-strength vortex pair diverged to two different states. The divergence reflected how one vortex deformed more than the other. The deformation difference is controlled by the unequal induced strain independent of viscous effects. The eccentricity plots at different Reynolds numbers $(6660, 13340$ and $20000)$ of two Λ values -0.415 and -1.0 are shown in figure 8. For reference, the $\Lambda = -1.0$ case is plotted which has identical results for both vortices over time. The eccentricities of all vortices converged to a unique state which was independent of Reynolds number. This was consistent with the finding of the previous work on equal-strength vortex pair (Sipp *et al.* [11] and Le Dizès and Verga [6]).

The oscillation frequency was found to be a function of viscosity. All four curves show the same behavior. The eccentricity oscillation amplitude about the mean value appears to be affected by the induced strain or the vortex circulation. The induced strain experienced by the negative vortex is identical initially for all Λ. The negative vortex circulation decreases when Λ is increased toward -0.1 from -1.0. The oscillation amplitude in figure 8(a) is greater and the oscillation wavelength is longer for the vortex with a weaker circulation.

On the other hand, the positive circulation was identical initially for the positive vortex, but the induced strain varied with Λ. In figure 8(b), the eccentricity oscillation has a bigger am-

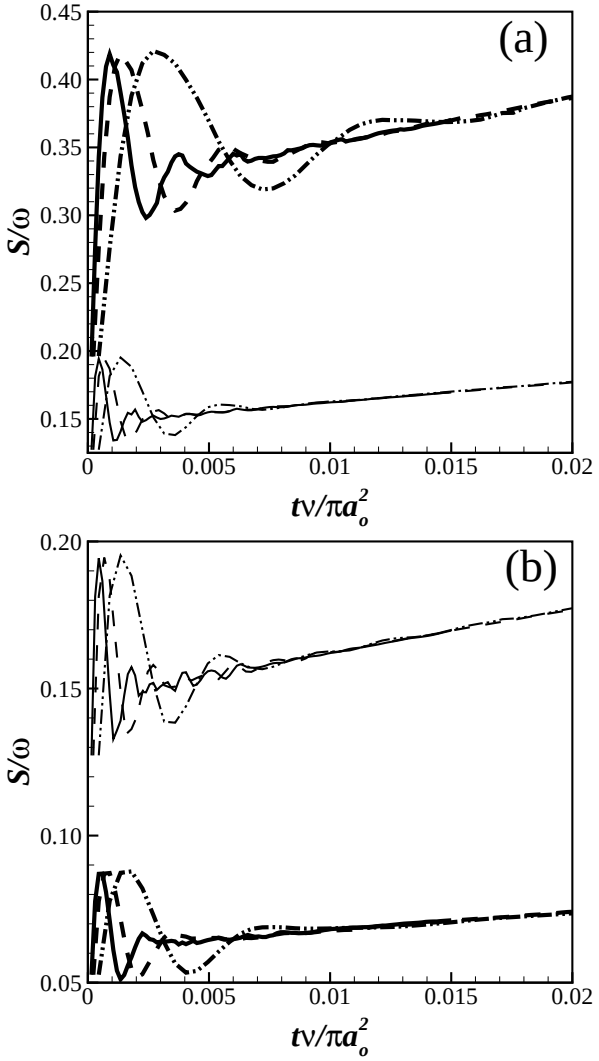

Figure 8: Eccentricity plotted against the viscous time scale. (a) Negative vortex (b) Positive vortex. $\Lambda = -0.415$ (thick) & -1 (thin). $Re = 20000$ (solid), 13340 (dash) & 6660 (double-dot)

plitude when the induced strain is stronger but the oscillation wavelength is shorter. The positive vortex under a weaker induced strain oppositely has a longer wavelength oscillation but smaller magnitude.

As the viscosity affected the flow at all times, the circulation and the induced strain should decay with an equal rate. Thus the positive vortex circulation equates to the induced strain on the negative vortex when Λ was varied.

Conclusions

Unequal strength counter-rotating vortex pairs have been investigated two-dimensionally using a spectral element method. The vortex pair relative strength, Λ, was varied from -1.0 to -0.1. Simulations have been carried out at three Reynolds numbers: 6660, 13340 and 20000 (based on the circulation).

The unequal strength vortex pair interaction was shown to be dependent on Λ. The difference of the induced strain on each vortex caused the vortices to evolve with distinct time scales and deform at different magnitudes. Eccentricity was defined to represent that magnitude. For an unequal vortex pair, the negative (weaker) vortex required more time than the positive (stronger) vortex to settle and the interaction dynamics is also stronger. However, the final states of the vortices were independent of the Reynolds number, and the converged vortex pair structure was only dependent on the initial spacing ratio and the Λ.

An evolution of $\Lambda = -0.415$ vortex pair at $Re = 13340$ was shown. The positive vortex was found to have a higher vorticity decay rate than the negative vortex. The principal strain direction in was observed to have a slight variation at the beginning of the simulations and settled to about $\pm 45^\circ$ orientation later on with respect to the a line joining two vortices.

Acknowledgements

The authors like to thank the Dept. of Mechanical Engineering and the Fluids Laboratory for Aeronautical and Industrial Research (FLAIR) of Monash University for providing all necessary resources in this investigation.

Joine So thankfully acknowledges the financial support of the Monash Department Scholarship (MDS) from the Dept. of Mechanical Engineering of Monash University to conduct this research.

References

[1] Batchelor, G.H., Axial flow in trailing line vortices, *J. Fluid Mech.*, 1964, *vol.***20**, 645–658.

[2] BristoL, R.L., Ortega, J.M., Marcus, P.S., and Şavas, ö., On cooperative instabilities of parallel vortex pairs, *J. Fluid Mech.*, 2004, *vol.***517**, 331–358.

[3] Lacaze, L., Ryan. K, and Le Dizés, S., Elliptic instability in a strained Batchelor vortex, *J. Fluid Mech.*, 2007, *vol.***577**, 345–361.

[4] Laporte, F. and Corjon, A. Direct numerical simulations of the elliptic instability of a vortex pair, *Physics of Fluids*, 2000, *vol.***12**, 1016–1031.

[5] Leweke, T. and Williamson, C.H.K., Cooperative elliptic instability of a vortex pair, *J. Fluid Mech.*, 1998, *vol.***360**, 85–119.

[6] Le Dizés, S. and Verga, A., Viscous interactions of two co-rotating vortices before merging, *J. Fluid Mech.*, 2002, *vol.***467**, 389–410.

[7] Karniadakis, G.E., Israfeli, M., and Orszag, S.A., Spectral Element - Fourier methods for incompressible turbulent flows, *Journal of Computational Physics*, 1991, *vol.***97**, 414–443.

[8] Meunier, P., Ehrenstein, U., Leweke, T. and Rossi, M., A merging criterion for two-dimensional co-rotating vortices, *Physics of Fluids*, 2002, *vol.***14**, 2757–2766.

[9] Moore, D.W. and Saffman, P.G., The instability of a straight vortex filament in a strain field, *Proc. R. Soc. London*, 1975, *Ser.***346**, 413.

[10] Ortega, J.M., BristoL, R.L., and Şavas, ö., Experimental study of the instbaility of unequal-strength counter-rotating vortex paris, *J. Fluid Mech.*, 2003, *vol.***474**, 35–84.

[11] Sipp, D., Jacquin, L. and Cosssu, C., Self-adaptation and viscous selection in concentrated two-dimensional dipoles, *Physics of Fluids*, 2000, *vol.***12**, 245–248.

[12] Ting, L. and Klein, R., *Viscous Vortical Flows*, Lecure Notes in Physics (Springer-Verlag, Berlin, 1991).